Received December 16, 2019, accepted December 29, 2019, date of publication January 23, 2020, date of current version February 4, 2020.

Digital Object Identifier 10.1109/ACCESS.2020.2968915

Rotordynamic Simulation Method of Induction Motors Including the Effects of Unbalanced Magnetic Pull

HEESOO KIM[1], JANNE NERG[2], (Senior Member, IEEE), TUHIN CHOUDHURY[1], AND JUSSI T. SOPANEN[1], (Member, IEEE)

[1]Department of Mechanical Engineering, LUT University, 53850 Lappeenranta, Finland
[2]Department of Electrical Engineering, LUT University, 53850 Lappeenranta, Finland

Corresponding author: Heesoo Kim (heesoo.kim@lut.fi)

This work was supported by the LUT Doctoral School Funding.

ABSTRACT This paper presents an optimal method for rotordynamic simulation of induction motors, including the effects of unbalanced magnetic pull (UMP). The developed simulation method containing the UMP model is simple but still accurate for the actual design process of induction motors. The UMP model is simplified by using the magnetizing current without calculation of the rotor current. The effects of the slot opening and saturation are initially incorporated into the model by using the Carter factor. To improve the accuracy of the model, the magnetizing current is calculated by the finite element analysis (FEA), and the proposed correction factor is also built into the model. Moreover, mixed eccentricity is modeled and applied to the time step rotordynamic simulation for considering the actual rotor eccentricity condition. Based on the developed UMP and eccentricity models, rotordynamic simulation methods within the induction motor design process are proposed and tested in a standard four-pole induction motor. The simulation results show that inclusion of the UMP force reduces the critical speeds and generates electromagnetic excitation. The study further shows that the effects of UMP vary with a change in static eccentricity, dynamic eccentricity, slip, and bearing stiffness. Finally, based on the results, a utilization plan of the developed methods is proposed.

INDEX TERMS Induction motor, mixed eccentricity, rotordynamics, unbalanced magnetic pull.

NOMENCLATURE

B_δ	Air-gap magnetic flux density.
$\mathbf{C}$	Damping matrix.
c	Correction factor.
e_{dy}	Amplitude of dynamic eccentricity.
e_{mix}	Amplitude of mixed eccentricity.
e_{st}	Amplitude of static eccentricity.
F	Magnetomotive force.
$\mathbf{F}_{\mathrm{g}}$	Gravity force matrix.
$\mathbf{F}_{\mathrm{ub}}$	Unbalance force matrix.
$\mathbf{F}_{\mathrm{ump}}$	UMP force matrix.
F_{x}	Net UMP force in horizontal direction.
F_{y}	Net UMP force in vertical direction.
$\mathbf{G}$	Gyroscopic matrix.
I_{m}	Magnetizing current.
$\mathbf{K}$	Stiffness matrix.
$k_{\mathrm{C,s}}$	Carter factor for stator.
$k_{\mathrm{C,r}}$	Carter factor for rotor.
$k_{\mathrm{C,tot}}$	Total Carter factor.
$\mathbf{K}_{\mathrm{ump}}$	UMP stiffness matrix.
l_{st}	Stator stack length.
$\mathbf{M}$	Mass matrix.
N	Number of turns in a winding.
n	Degree of polynomial.
p	Pole pair number.
$\mathbf{q}$	Displacement vector.
$\dot{\mathbf{q}}$	Velocity vector.
$\ddot{\mathbf{q}}$	Acceleration vector.
r	Air-gap radius.
w_ν	Winding factor.
t	Time variable.
x_{st}	x coordinate of static eccentricity.

The associate editor coordinating the review of this manuscript and approving it for publication was Xiaodong Sun.

x_1-y_1	Stator reference coordinate system.
x_2-y_2	Reference coordinate system with the bearing center as origin.
y_{st}	y coordinate of static eccentricity.
α	Circumferential location of the air gap on the rotor surface.
δ	Air-gap length.
δ_0	Mean air-gap length.
δ_0'	Equivalent mean air-gap length.
δ_0''	Equivalent mean air-gap length multiplied by correction factor.
ε_{mix}	Relative mixed eccentricity.
θ_{dy}	Direction angle of dynamic eccentricity.
θ_{mix}	Direction angle of mixed eccentricity.
θ_{st}	Direction angle of static eccentricity.
Λ	Air-gap permeance.
μ_0	Air permeance.
v	Harmonic order.
Ω	Rotor angular velocity.
Ω_n	First critical speed of the rotor.
ω	Electric angular velocity.

I. INTRODUCTION

In electrical machines, unbalanced magnetic pull (UMP) is unavoidable as it results from factors such as manufacturing tolerances and machine vibration. From the viewpoint of rotordynamics, the UMP results in additional vibration and bearing wear of the rotor system, which are critical for the stability and service life of the machine. These effects are gaining interest owing to the increase in the demand for high-speed and high-performance electrical machines. Therefore, a simulation method including the UMP effect on rotordynamics is required in the electrical machine design process.

The UMP results from an asymmetric air-gap magnetic flux density distribution between the rotor and the stator. Therefore, it is important to accurately simulate this distribution in the air-gap eccentricity condition. The generation principle of the air-gap magnetic flux varies depending on the type of electrical machine. This study focuses on the induction motor, which is the most widely used electrical machine type in industrial applications owing to its simple structure and low manufacturing cost. However, the process of UMP calculation in an induction motor is more complicated than in other types of electrical machines, such as traditional permanent magnet synchronous machines [1] or permanent magnet bearingless machines [2]–[4]. This is because the induction motor has a secondary circuit, where the rotor magnetic flux must be calculated. Moreover, the effect of parallel circuits in the cage rotor and the stator winding must be considered.

For the calculation of the UMP in an induction motor, two common approaches are the analytical method and the numerical method. The numerical method is based on the finite element analysis (FEA). Based on these two approaches, various attempts have been made to find appropriate solutions. Dorrell *et al.* [5], [6] studied an analytical method for calculating UMP caused by static, dynamic, and axial-varying eccentricity in a cage induction motor. In particular, they incorporated the rotor differential flux into their model. Tenhunen *et al.* [7] solved the magnetic field by the FEA and calculated the forces by applying a method based on the principle of virtual work. The force was measured using an Active Magnetic Bearing (AMB) system and compared with results obtained by using the principle of virtual work. They developed an impulse method for calculating the frequency response of the electromagnetic force on whirling cage rotors [8] and studied the effects of equalizing currents [9] and saturation [10] on the magnetic force. By using this method, they found that equalizing currents in both parallel branches in the stator winding and the rotor cage reduce the amplitude of the magnetic force. Holopainen *et al.* [11] developed an electromechanical rotor model including the electromagnetic force caused by arbitrary rotor motion in cage induction motors and estimated the parameters in the model by using the impulse method. Frauman *et al.* [12] studied the effect of slot harmonics in induction motors by using the impulse method. They found that the force components caused by slot harmonics increase with slip, and they can be reduced by increasing the number of rotor slots. Silwal *et al.* [13] studied the electromagnetic force and damping in a cage induction machine with dynamic eccentricity using the Power Balance Method (PBM) implemented in the FEA and evaluated the prospects and limitations of this method. A fast simulation method was introduced by Han and Palazzolo [14], who proposed a simplified magnetic equivalent circuit (MEC) model in 2D. The MEC is coupled with the motor electric model for transient simulation. Han *et al.* calculated UMP forces by the Maxwell stress tensor method, and the results were verified by comparing them with the FEA results.

The asymmetry of the air-gap magnetic flux density distribution is caused by several factors such as rotor eccentricity, diametrically asymmetric phase windings, and stator deformation and vibration. Moreover, the asymmetry is affected by slot harmonics and saturation of the magnetic circuit. This study focuses on the rotor eccentricity, which is the main factor from the viewpoint of rotordynamics. The rotor eccentricity is a result of several types of eccentricity; most studies address the UMP by considering conventional static and dynamic eccentricities. Dorrell [6] also modeled the UMP with axial-varying rotor eccentricity, and Di *et al.* [15] modeled the curved dynamic eccentricity caused by shaft bow, as the deflection of the shaft is an important and common problem in large electrical machines. They found that deflection produces an axial UMP force, which has an influence on the lifetime of the thrust bearings.

Overall, the literature review shows that various methods for estimation of UMP forces were studied. Nevertheless, the existing methods are still not suitable for rotordynamic simulation. The numerical method based on FEA can achieve accurate results by taking into account the saturation of the magnetic circuit and the flux leakage as well as the effect of rotor/stator slotting. On the other hand, the main drawback

of this method is its high computational cost especially for dynamic eccentricity simulation. The analytical method, in contrast, does not have a high computational cost; however, it is difficult to take all the factors into consideration in the analysis. In addition, the existing methods calculate UMP forces by static and dynamic eccentricity separately. This is different from an actual rotor eccentricity condition, where static and dynamic eccentricities are present simultaneously. Therefore, a special and optimized method for rotordynamic simulation by considering both the UMP calculation and the rotordynamic simulation process is required.

In this study, an optimal method for rotordynamic simulation of induction motors including UMP is developed, which is simplified but still accurate for the actual design process of induction motors. The developed method is based on an analytical UMP force equation, and it uses the magnetizing current without separate calculations of the stator and rotor magnetic fluxes on the grounds that the magnetizing current is nearly constant regardless of the speed change in the constant load condition [16]. Moreover, to improve the accuracy of the effect of slot opening, saturation, flux leakage, and load variation, two parameters are used:

- Magnetizing current, calculated by the FEA
- A novel correction factor, inversely calculated from the UMP force, which is estimated by the FEA

By this process, the accuracy of the UMP force calculation is improved, yet the computational cost is not significantly increased. Finally, by a combination of the proposed mixed eccentricity model and the time step rotordynamic simulation concept, a rotordynamic simulation method considering simultaneously the static and dynamic eccentricity is obtained. Based on these methods, a rotordynamic simulation process in the induction motor design is suggested.

For validation of the developed methods, the simulation was conducted for a 30 kW four-pole induction motor, and the results obtained from the variation of static eccentricity, dynamic eccentricity, slip, and bearing stiffness showed the effects of the UMP on the rotordynamics of an induction motor.

II. SIMULATION METHOD INCLUDING THE UMP CALCULATION

In this section, a simulation method is developed to determine the rotordynamic characteristics of an induction motor affected by the UMP. First, mixed air-gap eccentricity is modeled employing the concept of time step simulation. Then, an analytical UMP force equation is established based on the eccentricity modeling. The accuracy of the analytical UMP calculation is improved by using the results obtained by the FEA. Finally, the rotordynamic simulation process including UMP calculation within the overall design process of an induction motor is presented.

A. MIXED ROTOR ECCENTRICITY MODELING FOR TIME STEP ROTORDYNAMIC SIMULATION

Prior to UMP modeling, the concept of air-gap eccentricity has to be defined and delineated because the rotordynamic simulation method including UMP calculation depends on the eccentricity model. This study considers static eccentricity and dynamic eccentricity simultaneously. Therefore, a mixed eccentricity model is defined by using the method studied in the previous research [1]. In this model, the dynamic eccentricity has a time-dependent term because it is defined from actual rotor behavior; however, in each time step, it can be considered a static condition calculated from the instantaneous location of the rotor. Consequently, the mixed eccentricity can be considered a static condition in each time step, and thus, the UMP can be modeled without separate definitions for static and dynamic eccentricity in the following section.

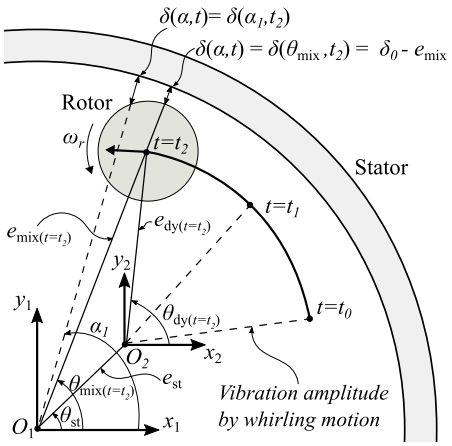

FIGURE 1. Mixed eccentricity model for the time step analysis.

Fig. 1 explains the concept of mixed eccentricity. First, a new reference coordinate system is defined by parallel translation of the x_1-y_1 stator reference coordinate system as the same degree as the static eccentricity. Here, static eccentricity is defined by its amplitude e_{st} and direction angle θ_{st} as the initial constant condition. The bearing center can be considered to be the origin of the newly defined x_2-y_2 reference coordinate system, i.e., the origin of dynamic eccentricity. Thus, dynamic eccentricity is defined in x_2-y_2 reference coordinates by its time-dependent amplitude $e_{dy}(t)$ and direction angle $\theta_{dy}(t)$, which are calculated from the whirling motion of the rotor. Consequently, mixed eccentricity can be defined as the amplitude e_{mix} and the direction angle θ_{mix} by (1) and (3) established with the amplitudes and direction angles of the static and dynamic eccentricities. Here, ε_{mix} is the relative mixed eccentricity, and δ_0 is the mean air-gap length.

$$e_{mix}(t) = \sqrt{\begin{aligned}&\left(e_{st}\cos\theta_{st} + e_{dy}(t)\cos\left(\theta_{dy}(t)\right)\right)^2 \\ &+ \left(e_{st}\sin\theta_{st} + e_{dy}(t)\sin\left(\theta_{dy}(t)\right)\right)^2\end{aligned}} \quad (1)$$

$$\varepsilon_{mix}(t) = \frac{e_{mix}(t)}{\delta_0} \quad (2)$$

$$\theta_{mix}(t) = \tan^{-1}\left(\frac{e_{st}\sin\theta_{st} + e_{dy}(t)\sin\left(\theta_{dy}(t)\right)}{e_{st}\cos\theta_{st} + e_{dy}(t)\cos\left(\theta_{dy}(t)\right)}\right) \quad (3)$$

B. UMP CALCULATION OF INDUCTION MOTORS IN THE STATIC ECCENTRICITY CONDITION

This section explains the UMP calculation method for rotordynamic simulation in the induction motor design process. Typically, a Campbell diagram is used to determine critical speeds, and a vibration response plot is employed to study variable excitations and their effect on vibration. However, a large number of calculations are required to obtain these results when using the time step simulation concept, which leads to a high computational cost. Therefore, it is necessary to develop an appropriate simulation model that ensures both the accuracy and a reasonable computation load. This study proposes a simplified UMP calculation model, while maintaining the accuracy of the rotordynamic analysis. The model uses the magnetizing current and the Carter factor with the following assumptions. The assumptions for the simplification of the UMP model are:

1) The magnetizing current, calculated in the concentric rotor, rated speed and rated load condition, is constant regardless of variation in the air-gap eccentricity and rotor speed. For a machine in which the load variation is not significant, this assumption is valid [16].
2) Stator/rotor slot opening, saturation, and flux leakage only have an effect on the magnitude of the UMP, not its time harmonics. Therefore, these effects can be taken into account in the UMP model by increasing the equivalent mean air-gap length.

In the following sections, the UMP calculation model is established within the assumption that mixed eccentricity is static at instantaneous time. The UMP variation caused by the time-dependent term of the dynamic eccentricity is considered in the time step rotordynamic simulation process.

1) ANALYTICAL CALCULATION OF AIR-GAP MAGNETIC FLUX DENSITY DISTRIBUTION

The asymmetry of the air-gap magnetic flux density distribution generates the UMP. Therefore, calculation of the air-gap magnetic flux density distribution is required, and it can be modeled in terms of rotating air-gap permeance harmonics and surface magnetomotive force (MMF) harmonics as

$$B_\delta(\alpha, t) = \mu_0 \frac{F(\alpha, t)}{\delta(\alpha, t)} = \Lambda(\alpha, t) F(\alpha, t). \tag{4}$$

Here, α is a variable for defining the circumferential location of the interested air gap on the rotor surface. It is presented as the relative angle from the centerline of a predetermined stator tooth, which coincides with the horizontal axis of the x_1-y_1 reference coordinates as in Fig. 1, and t denotes time. For the definition of the air gap permeance, the air gap length is first defined by (5) using the mixed eccentricity model. Unlike the existing conventional separate definitions, this equation can take into account static eccentricity and dynamic eccentricity simultaneously because it involves the time-dependent eccentricity and direction angle

$$\delta(\alpha, t) = \delta_0 \left\{1 - \varepsilon_{\text{mix}}(t) \cos\left(\alpha - \theta_{\text{mix}}(t)\right)\right\}. \tag{5}$$

Air-gap permeance is obtained by inverting the air-gap length and multiplying the air permeance μ_0. It can be approximated in a series form in the mixed eccentricity condition [17] and written as

$$\begin{aligned}\Lambda(\alpha, t) &= \frac{\mu_0}{\delta(\alpha, t)} = \frac{\mu_0}{\delta_0 \left\{1 - \varepsilon_{\text{mix}}(t) \cos\left(\alpha - \theta_{\text{mix}}(t)\right)\right\}} \\ &= \frac{\mu_0}{\delta_0} \sum_{m=0}^{\infty} \varepsilon_{\text{mix}}(t)^m \cos^m\left(\alpha - \theta_{\text{mix}}(t)\right) \\ &= \frac{\mu_0}{\delta_0 \sqrt{1 - \varepsilon_{\text{mix}}^2}} \left[1 + \sum_{m=1}^{\infty} 2 \left(\frac{1 - \sqrt{1 - \varepsilon_{\text{mix}}(t)^2}}{\varepsilon_{\text{mix}}(t)}\right)^m \right. \\ &\quad \left. \cos\left\{m\left(\alpha - \theta_{\text{mix}}(t)\right)\right\}\right]. \end{aligned} \tag{6}$$

When a three-phase symmetrical stator has three same windings shifted in space by $2\pi/3$ electrical degrees and it is fed with a balanced current system, the total MMF can be calculated by the magnetizing current I_{m} and harmonics series as [18]

$$F(\alpha, t) = \frac{3\sqrt{2}\, N I_m}{\pi p} \begin{bmatrix} w_{f1} \sin(\omega t - p\alpha) \\ + \dfrac{w_{f5}}{5} \sin(\omega t + 5p\alpha) \\ + \dfrac{w_{f7}}{7} \sin(\omega t - 7p\alpha) + \cdots \end{bmatrix}. \tag{7}$$

Here, w_{fv} is the winding factor ($v = 1, -5, 7$, etc.), which can be obtained by using the well-known method given in [19], N is the phase-winding number of turns, p is the pole pair number, and ω is the stator supply frequency. Generally, magnetizing current is calculated analytically in the electromagnetic design in the induction motor design process.

Thus, when the rotor has mixed eccentricity, the air-gap magnetic flux density distribution can be expressed as

$$\begin{aligned} &B_\delta(\alpha, t) \\ &= \frac{3\sqrt{2}\mu_0 N I_{\text{m}}}{\pi p \delta_0 \sqrt{1 - \varepsilon_{\text{mix}}(t)^2}} \\ &\quad \times \left[1 + 2 \sum_{m=0}^{\infty} \left(\frac{1 - \sqrt{1 - \varepsilon_{\text{mix}}(t)^2}}{\varepsilon_{\text{mix}}(t)}\right)^m \cos\left\{n\left(\alpha - \theta\right)\right\}\right] \\ &\quad \times \begin{bmatrix} w_{f1} \sin(\omega t - p\alpha) + \dfrac{w_{f5}}{5} \sin(\omega t + 5p\alpha) \\ + \dfrac{w_{f7}}{7} \sin(\omega t - 7p\alpha) + \cdots \end{bmatrix}. \end{aligned} \tag{8}$$

2) EFFECT OF SLOT OPENING ON THE AIR GAP MAGNETIC FIELD

The consideration of the air-gap magnetic field is based on the concept of a machine formed by two unslotted cylinders. However, in general, an induction motor has a slotted stator and rotor. Therefore, the next step is to consider the effect of slotting on the air-gap magnetic field.

This study takes into account the effect of slotting by using the Carter factor in the model. The analytical equations of the factor for different stator and rotor geometries are given in [19]. Here, the slot opening length is defined by adding a virtual slot opening resulting from the teeth oversaturation to the physical slot opening [18].

Thus, by obtaining the Carter factors for the stator ($k_{C,s}$) and rotor ($k_{C,r}$), the equivalent mean air-gap length is calculated as

$$\delta_0' = k_{C,s}k_{C,r}\delta_0 = k_{C,tot}\delta_0. \tag{9}$$

Here, $k_{C,tot}$ is the total Carter factor. Further, the updated relative mixed eccentricity is expressed by (10) by applying the Carter factor and the mixed eccentricity established in section II. A.

$$\varepsilon_{mix}' = \frac{e_{mix}}{\delta_0'} = \frac{e_{mix}}{k_{C,tot}\delta_0} \tag{10}$$

3) UMP FORCE AND LINEARIZED STIFFNESS

The UMP is calculated from the previously obtained air gap flux density distribution by using the Maxwell stress tensor method. The net UMP forces in the horizontal and vertical directions are calculated by integrating the Maxwell stress tensor in the air gap around the rotor surface as

$$\begin{aligned} F_x &= \int_0^{2\pi} \frac{(B_\delta(\alpha,t))^2}{2\mu_0} r l_{st} \cos\alpha d\alpha \\ F_y &= \int_0^{2\pi} \frac{(B_\delta(\alpha,t))^2}{2\mu_0} r l_{st} \sin\alpha d\alpha. \end{aligned} \tag{11}$$

Here, r is the air-gap radius and l_{st} is the length of the stator stack.

By using the obtained UMP force equation, the UMP stiffnesses in the horizontal and vertical directions are linearized around the static eccentricity point (x_{st}, y_{st}) as

$$k_{ump,x} \approx \left.\frac{dF_x}{dx}\right|_{x=x_{st}}, k_{ump,y} \approx \left.\frac{dF_y}{dy}\right|_{y=y_{st}}. \tag{12}$$

4) IMPROVEMENT OF THE ANALYTICAL UMP CALCULATION BY COMBINING IT WITH THE FEA

In the established UMP force equation, the magnitude of the UMP force depends on the magnetizing current and the Carter factor. However, in the analytical estimation of these values, an error is inevitable because of the assumptions made in the analytical calculation process. For example, a varying load slightly changes the magnetizing current, but it is assumed to be a constant in the analytical calculation. Moreover, the model does not include the effects of saturation and flux leakage. Therefore, this section focuses on improving the accuracy of the analytical calculation by combining it with the FEA-based approach. First, the magnetizing currents are estimated in several load cases by calculating the air gap magnetic fluxes by the FEA. Unlike analytical calculation, this calculation takes account of the variation in the magnetizing current caused by a change in load. Second, as all the remaining effects cannot be considered by an analytical model with the Carter factor only, a new load/eccentricity-dependent correction factor c is introduced, and it is multiplied by the equivalent air-gap length. The updated equivalent mean air-gap length is obtained as

$$\delta_0'' = c \cdot k_{C,tot}\delta_0. \tag{13}$$

To obtain this correction factor, UMP forces for several eccentricity cases in the eccentricity range under study are obtained by the FEA within certain load condition. Then, by using the FEA-calculated UMP forces in the selected eccentricity cases and the analytical UMP force equation established in the previous section, the correction factors are inversely calculated for every selected eccentricity cases. Furthermore, by using polynomial curve fitting, the function for the correction factor in the eccentricity range under study can be obtained as

$$c = \sum_{i=1}^{n} a_i \varepsilon^n + a_{n+1}. \tag{14}$$

Here, n = degrees of polynomial < number of the FEA-calculated cases at different eccentricities. The correction factor function is calculated for all load cases individually.

Finally, the UMP force equation is revised by substituting the updated magnetizing current and applying the updated equivalent air-gap length. This revised equation calculates UMP force magnitudes that are close to the FEA-calculated UMP force values. On the other hand, the simulation time is not significantly increased, and therefore, an improved but computationally efficient rotordynamic simulation method is achieved.

C. MODELING OF ROTOR–BEARING SYSTEM WITH UMP

In the rotor-bearing system model of the induction motor, the UMP is considered with two different approaches.

First, the UMP is applied as an external force to the electrical rotor, and the equation of motion is expressed as

$$\mathbf{M}\ddot{\mathbf{q}} + (\mathbf{C} + \Omega\mathbf{G})\dot{\mathbf{q}} + \mathbf{K}\mathbf{q} = \mathbf{F}_{ub} + \mathbf{F}_g + \mathbf{F}_{ump} \tag{15}$$

where $\mathbf{q}$ is the displacement vector, and $\mathbf{M}$, $\mathbf{C}$, $\mathbf{G}$, and $\mathbf{K}$ are the mass, damping, gyroscopic, and stiffness matrices, respectively. The term Ω is the rotor angular velocity. $\mathbf{F}_{ub}$, $\mathbf{F}_{ump}$, and $\mathbf{F}_g$ are the unbalance force, the UMP force, and the gravity force matrices, respectively.

Second, the UMP is applied as a linearized negative stiffness spring. The equation of motion with UMP can be established using the UMP stiffness matrix $\mathbf{K}_{ump}$, linearized around a given static eccentricity as

$$\mathbf{M}\ddot{\mathbf{q}} + (\mathbf{C} + \Omega\mathbf{G})\dot{\mathbf{q}} + (\mathbf{K} - \mathbf{K}_{ump})\mathbf{q} = \mathbf{F}_{ub} + \mathbf{F}_g. \tag{16}$$

D. ROTORDYNAMIC SIMULATION METHODS WITHIN THE INDUCTION MOTOR DESIGN PROCESS

By applying the above-discussed UMP calculation methods and the rotor-bearing system model, the rotordynamic simulation process including the UMP is established in the induction motor design process and presented in Fig. 2 as a flowchart.

According to the design process of an induction motor, the stator and rotor dimensions are determined initially by analytical electromagnetic calculations. In this stage, the magnetizing current and the Carter factor are determined

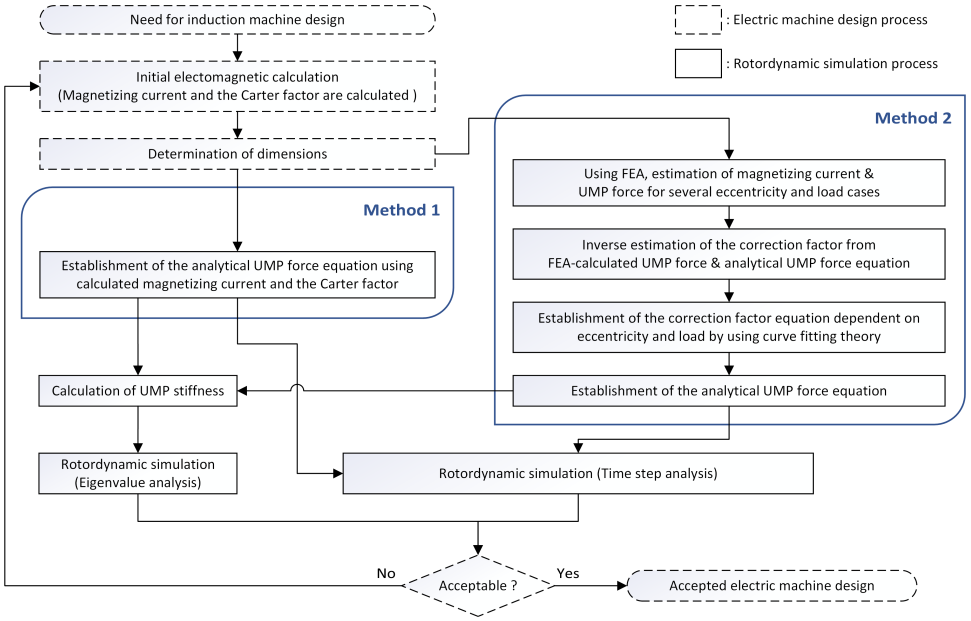

FIGURE 2. Flowchart of the proposed rotordynamic simulation processes considering UMP in the electrical machine design process.

for a concentric rotor in the rated rotor speed and load condition. These values are used in the analytical equation for calculating UMP (see Method 1 in the flowchart of Fig. 2). In the improved method (Method 2), a load-dependent magnetizing current function and a load/eccentricity-dependent Carter factor function are obtained by using the improved process presented in the previous section. By using the updated magnetizing current and the Carter factor functions, the equation applied in Method 1 for UMP calculation is updated.

The obtained UMP force equation is applied to the rotor–bearing system model as a nonlinear external force. Then, this equation of motion is solved by the time step analysis by applying a numerical integration method, which is performed by using the ode15s function in MATLAB. This time-transient analysis is conducted for a certain rotor speed and eccentricity case by the following process. First, the mixed eccentricity at a time step is calculated by using the rotor displacement obtained at the previous time step by (1)–(3) in section II. A, and then, the UMP force is calculated by using the model presented in section II. B. With the same process, the rotor displacement and the UMP force are updated at every time step, and the rotor motion is obtained until the motion reaches a steady state. Finally, the steady-state motion is selected as the result. The same simulation process is repeated for different rotor speed and eccentricity cases.

To determine the effects of static eccentricity and dynamic eccentricity separately, two eccentricity types are controlled independently. Static eccentricity is controlled as an initial constant value in the eccentricity model. However, dynamic eccentricity cannot be defined as an initial constant value because it depends on the rotor whirling motion, which is a result of simulation at every time step. Meanwhile, it is a valid assumption that in a linear system, at a constant speed, the response amplitude increases linearly as a function of unbalance mass. Hence, in this study, the dynamic eccentricity is controlled by the magnitude of the unbalance mass.

A simple alternative to the time step simulation is to solve the motion equation with a linearized UMP spring model using an eigenvalue analysis. The UMP stiffness can be obtained from the previously established UMP force equation by linearization around a given static eccentricity. This is a simple and fast method for the rotordynamic analysis. The applicability of the method is investigated by comparing it with the results obtained by the time step simulation.

III. SIMULATION RESULT

To investigate the effect of UMP on the rotordynamics of an induction motor, rotordynamic simulation is conducted for a common 30 kW squirrel cage induction motor. The simulation model is designed to obtain steady-state rotor motion at each rotational speed in the presence of mixed rotor eccentricity. By interpreting the change in the rotor motion by varying several factors such as static eccentricity, dynamic eccentricity, slip, and bearing stiffness, the effect of UMP is determined. Furthermore, the results are compared with the results reported elsewhere in the literature [6], [20] to verify the simulation method.

A. INDUCTION MOTOR UNDER STUDY AND ITS FEA ROTOR MODEL

Table 1 lists the parameters of the 30 kW squirrel cage induction motor under study. The rotor part of the motor is modeled with beam finite elements as shown in Fig. 3. The model has four degrees of freedom per node, and it is assumed

TABLE 1. Parameters of the induction motor under study.

Symbol	Quantity	Values (Unit)
P	rated power	30 kW
n	rated speed	1473 rpm
U	rated phase-to-phase voltage	690 V
I	rated current	32.5 A
s	rated slip	0.18
p	number of pole pairs	2
m	number of phases	3
N	number of series turns per phase	104
Q_s	number of stator slots	48
J	number of rotor bars	36
δ_0	mean air-gap length	0.8 mm
D_r	rotor outer diameter	214 mm
l	stack length	205 mm
$K_{bearing}$	bearing stiffness	$8.1{\cdot}10^7$ N/m (DE) [a] $9.6{\cdot}10^7$ N/m (NDE) [a]
$C_{bearing}$	bearing damping	$2.0{\cdot}10^3$ N/m (DE) $2.4{\cdot}10^3$ N/m (NDE)

[a]DE = Drive End, NDE = Non-Drive End.

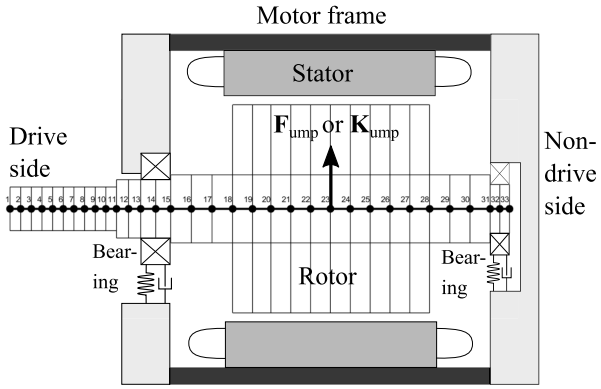

FIGURE 3. Motor structure and finite element model of the rotor system under study.

that there is no displacement in the axial direction and no rotation around the rotor axis. The rotor is supported by two deep groove ball bearings (6312/C3 on the drive side and 6210/C3 on the non-drive side). The bearing stiffness values ($K_{bearing}$) are estimated by using a simple method proposed by Gargiulo [21], and the bearing damping values are estimated as $2.5{\cdot}10^{-5} \cdot K_{bearing}$ [22]. The UMP is applied to the rotor by using two different approaches (external force or linear spring) at node 23 located in the middle of the electrical rotor as shown in Fig. 3. Thus, axial distribution of the UMP force is not considered in this model.

B. UMP CALCULATION BY TWO METHODS AND ITS COMPARISON WITH THE FEA RESULTS

For verification of the developed UMP calculation methods, air-gap magnetic flux density distributions and UMP force are calculated for the induction motor under study by using Methods 1 and 2 presented in section II. B. This is followed by a comparison with the FEA-based results.

In Method 1, the magnetizing current, the Carter factor, and the UMP force are obtained by analytical calculations only. On the other hand, in Method 2, FEA results are required. Therefore, a two-dimensional time-stepping electromagnetic FEA was performed in different load conditions and at different eccentricities. First, the magnetizing current, in each of the studied load conditions with a centered rotor, was calculated by using the FEA. Second, a set of FEA calculations were performed to obtain the UMP force in different load conditions and at different static eccentricities. The correction factor function for all interested eccentricity and load conditions is calculated inversely from the FEA-calculated UMP force. This correction factor function and the newly calculated magnetizing current are used to obtain the improved UMP force equation. Table 2 presents the results obtained by the FEA and the analytical Methods 1 and 2. Here, Method 2 is simply the process for updating the analytical UMP force equation to get the same UMP force with the FEA results. Therefore, the results calculated by Method 2 are equal to the FEA results.

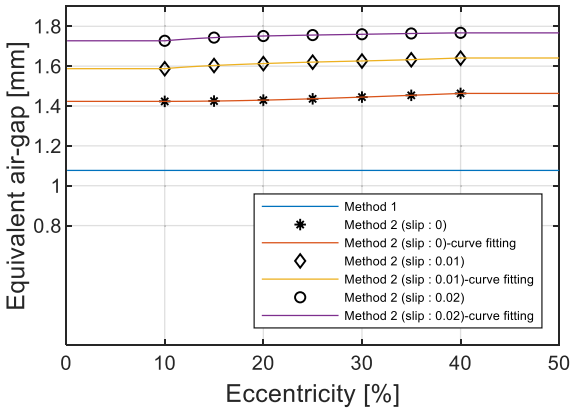

FIGURE 4. Equivalent mean air-gap length calculated by Method 1 and 2.

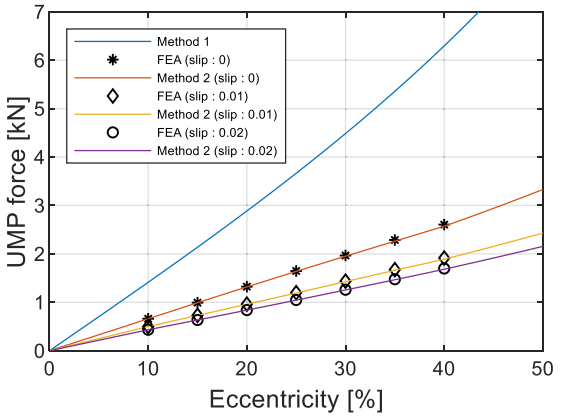

FIGURE 5. Comparison of UMP forces calculated by Methods 1, 2, and FEA.

Figs. 4 and 5 show the equivalent mean air-gap length and UMP force by varying eccentricity for different cases of calculation method and slip. Here, in the case of small eccentricity (<10%), it is assumed that the correction factor is the same as with the 10% eccentricity because the

TABLE 2. UMP force comparison between analytical methods 1,2, and FEA.

ε (%)	Method 2 (F_{ump} is same with FEA-calculated value.)									Method 1 (I_m : 10.53 A)			
	slip : 0 (I_m : 10.95 A)			slip : 0.01 (I_m : 11.22 A)			slip : 0.02 (I_m : 11.87 A)						
	F_{ump} (N)	$c{\cdot}k_c$	k_{ump} (N/m)	F_{ump} (N)	$c{\cdot}k_c$	k_{ump} (N/m)	F_{ump} (N)	$c{\cdot}k_c$	k_{ump} (N/m)	F_{ump} (N)	Error [a] (%)	k_c	k_{ump} (N/m)
10	660.1	1.779	$8.31{\cdot}10^6$	498.6	1.984	$6.28{\cdot}10^6$	432.9	2.159	$5.44{\cdot}10^6$	1412.6	226	1.346	$1.79{\cdot}10^7$
15	992.4	1.781	$8.40{\cdot}10^6$	729.7	2.004	$6.16{\cdot}10^6$	634.5	2.179	$5.35{\cdot}10^6$	2137.4	237	"	$1.84{\cdot}10^7$
20	1322.4	1.787	$8.50{\cdot}10^6$	961.9	2.016	$6.15{\cdot}10^6$	839.4	2.189	$5.35{\cdot}10^6$	2885.0	244	"	$1.90{\cdot}10^7$
25	1646.3	1.795	$8.59{\cdot}10^6$	1197.9	2.025	$6.19{\cdot}10^6$	1047.6	2.195	$5.39{\cdot}10^6$	3664.2	250	"	$2.00{\cdot}10^7$
30	1966.3	1.806	$8.71{\cdot}10^6$	1435.8	2.032	$6.27{\cdot}10^6$	1259.3	2.200	$5.47{\cdot}10^6$	4484.5	256	"	$2.11{\cdot}10^7$
35	2286.7	1.817	$8.85{\cdot}10^6$	1674.3	2.040	$6.38{\cdot}10^6$	1475.9	2.205	$5.57{\cdot}10^6$	5357.1	263	"	$2.26{\cdot}10^7$
40	2603.7	1.829	$9.04{\cdot}10^6$	1913.9	2.050	$6.49{\cdot}10^6$	1697.8	2.209	$5.70{\cdot}10^6$	6294.7	271	"	$2.44{\cdot}10^7$

[a]The difference between UMP forces by the FEA in the 0.02 slip case and Method 1 is expressed as a percentage error.

FEA-calculated UMP force can have a significant error at a small eccentricity. Fig. 5 shows that the UMP force calculated by using the purely analytical Method 1 is much larger than the results obtained by the FEA. Most probably, this is explained by the fact that the analytical calculation method cannot accurately simulate all the effects of saturation, slot opening, and flux leakage. Thus, in Method 2, the UMP force equation is updated by using the correction factor calculated inversely from the FEA result. Fig. 5 shows that when the slip increases toward the rated value, the UMP force decreases, which is in agreement with the measured results in [6]. When using Method 2, although the magnetizing current increases with an increase in slip, the same trend is observed with an increase in the equivalent mean air-gap length (Fig. 4).

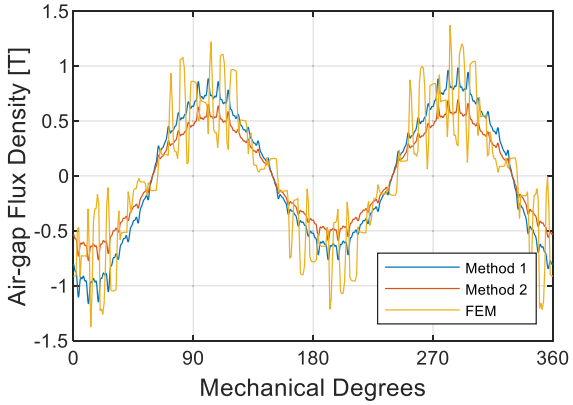

FIGURE 6. Air-gap flux density distributions in the 30% eccentricity condition.

Fig. 6 depicts the calculated air-gap magnetic flux density distributions at the 30 % eccentricity. A comparison between the methods reveals that the fundamental distributions are quite similar, but there is a difference in the magnitudes of higher harmonics. In the FEA result, the magnitude of higher harmonics is greater than in the analytical results. This deviation is probably caused by the slot openings of both the stator and the rotor. In the FEM result, the slot opening effect is shown as a fluctuation at every slot in the model, whereas in the analytical result, this effect is considered by reducing the magnetic flux density based on the Carter factor.

In the rotordynamic analysis at each time step, if the resultant UMP force by the analytical model is in agreement with the FEA result, the error in space distribution of the air gap magnetic flux density does not have an influence on the rotordynamic result because only the total resultant UMP force having a certain direction is applied to the rotor. Thus, it can be concluded that developed UMP model is suitable for the rotordynamic analysis. Whereas, the effect of UMP on the rotordynamics is more dependent on the time-dependent variation in the direction and amplitude of the UMP force.

C. SIMULATION PLAN FOR DETERMINING THE EFFECT OF UMP

Previous studies show that UMP affects the rotordynamics mainly in two ways; first, by a reduction in the critical speed as a result of a negative stiffness effect, and second, by generating additional vibration excitations. To investigate these two effects on the rotordynamic behavior, the vibration response of the rotor is obtained in the speed range from 500 rpm to 20,000 rpm. Normal speed steps of 100 rpm with 10 rpm steps close to the peak response points are applied and plotted by collecting the overall vibration amplitude (measured at node 23) of the rotor for every speed step. This speed range is optimal for detecting the UMP effect associated with the critical speed. Here, the first critical speed Ω_n of the rotor under study is at 15,100 rpm without the consideration of UMP.

The condition for reference simulation including the UMP effect is such that the slip is 0.02, the static eccentricity is 30 %, the unbalance mass is 960 g·mm, the bearing stiffnesses are $8.1{\cdot}10^7$ N/m (Drive end) and $9.6{\cdot}10^7$ N/m (Non-drive end), and the simulation method is Method 2 with the time step analysis. By studying the vibration responses while varying the conditions individually, the effect of each parameter can be observed. First, the responses for the five different static eccentricity cases: 0 %, 10 %, 20 %, 30 %, and 40 % are obtained to determine the effect of variation in the static eccentricity. Second, the responses for the three different unbalance mass cases: 480 g·mm, 960 g·mm, and 1,920 g·mm are obtained to determine the effect of variation in the dynamic eccentricity. Third, the responses for the three different slip cases: 0 (No-load condition), 0.01, and 0.02 are

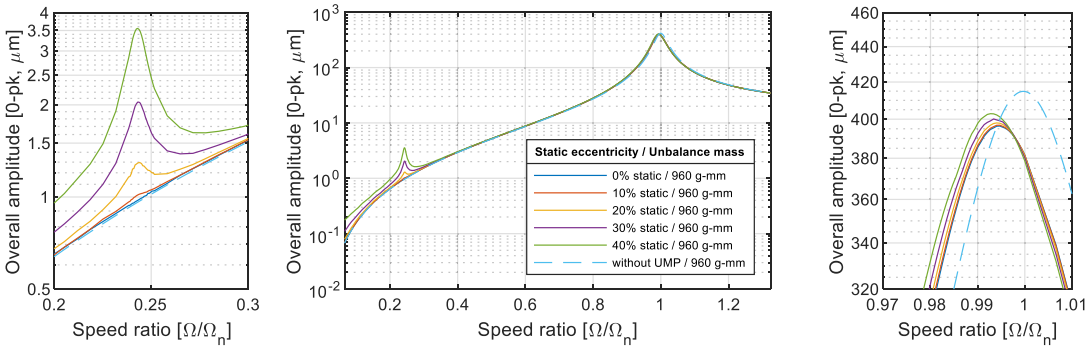

FIGURE 7. Vibration responses versus rotor speed in different static eccentricity cases using Method 2 (center figure), close-up near the 0.25 speed ratio (left), and close-up near the critical speed (right).

obtained to determine the effect of variation in slip, which can be regarded as the effect of variation in the load condition. Fourth, the responses for the three different bearing stiffness cases: $8.1{\cdot}10^7$ N/m (Drive end), $9.6{\cdot}10^7$ N/m (Non-drive end), and $5{\cdot}10^7$ N/m at both ends and $1{\cdot}10^7$ at both ends are obtained to determine the change in the UMP effect by varying the bearing stiffness. Finally, the responses for the three different simulation methods suggested in this study: Method 1 by using pure analytical calculation, Method 2 improved by the FEA, and adopting the linearized UMP spring coefficients from Method 1 and 2 are obtained to compare and discuss the usefulness of each method. Here, all responses including the UMP effect are compared with the result obtained without the UMP effect because the purpose of these simulations is to determine the effect of the UMP. In order to easily compare the rotor speed of the peak response with the critical speed, the rotor speed is expressed as the speed ratio to the first critical speed Ω_n (15,100 rpm) for the case without UMP.

Additionally, to determine the characteristics of the UMP excitations and the fundamental reason for the change in the vibration response, the rotor orbit and the Fast Fourier transform (FFT) of the displacement at one-fourth of the critical speed (rotor speed at which the resonance caused by twice the line frequency occurs) are obtained. To simultaneously determine the effect of slip, results for two slip cases, 0 and 0.02, are obtained and compared.

D. SIMULATION RESULTS AND DISCUSSION

Fig. 7 shows vibration responses in different static eccentricity cases. Two effects are apparent in the close-up figures around two response peaks: One is the effect on the rotor critical speed and the corresponding vibration amplitude, and the other is the effect of twice the line frequency excitation generated by the UMP force.

As to the first effect, a comparison of the results in the 0 % static eccentricity case (with dynamic eccentricity only) and the case without UMP shows that the reduction in the critical speed is mainly caused by dynamic eccentricity; according to the results, the critical speed decreases by 0.6 % due to the dynamic eccentricity. On the other hand, the reduction in the critical speed caused by static eccentricity is relatively small. When the static eccentricity is changed from 0 % to 40 %, the critical speed decreases only by 0.15 %. Moreover, according to the results, the vibration amplitude at the critical speed decreases by 0.06 % as a result of the dynamic eccentricity but it increases by 0.02 % when the static eccentricity is changed from 0 % to 40 %. The decrease in the amplitude caused by the dynamic eccentricity is mainly due to a decrease in the unbalance response, which, again, occurs as a result of a reduction in the critical speed. By contrast, the increase in the amplitude caused by the static eccentricity is a result of an increase in the magnitude of the UMP force.

As to the second effect, the results show that the static eccentricity produces a peak response at the 0.25 speed ratio (one fourth of the critical speed). This peak response results from twice the line frequency excitation which coincides with the mechanical natural frequency of the rotor. In the studied machine, twice the line frequency is equal to four times the speed frequency because it is a four-pole machine. Additionally, the vibration amplitude at the 0.25 speed ratio is increased by the static eccentricity. The reason for this is that the amplitude of the UMP increases with an increase in the static eccentricity. This result is in agreement with [20], where the generation of twice the line frequency vibration as a result of the UMP is explained. Fig. 11 shows the frequency component occurring as a result of this excitation in the FFT.

Fig. 8 presents the vibration responses in three cases of dynamic eccentricity. For the reference dynamic eccentricity (unbalance mass: 960 g·mm), the reduction in the critical speed is 0.66 %. When the dynamic eccentricity is two times the reference dynamic eccentricity, the corresponding critical speed reduction increases to 1.32 %. However, when it is half of the reference dynamic eccentricity, the corresponding critical speed reduction decreases to 0.53 %. It means that the critical speed reduction has a positive correlation with the dynamic eccentricity. Furthermore, theoretically, when the unbalance mass increases, both the centrifugal force and the UMP force caused by the dynamic eccentricity will increase. However, the close-up in Fig. 8 shows that the

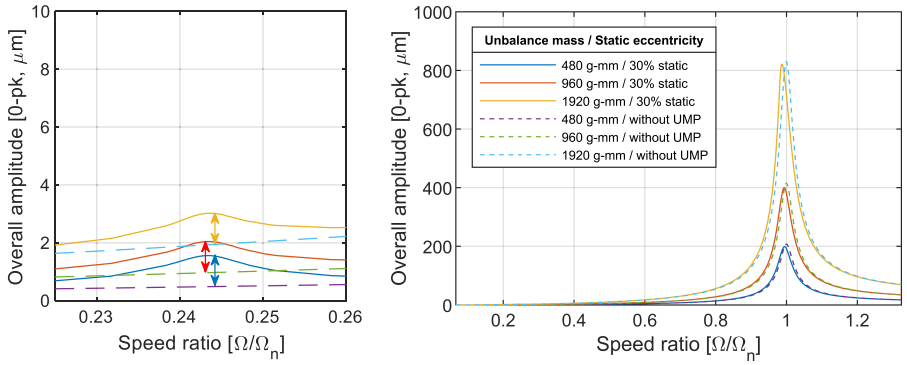

FIGURE 8. Vibration responses versus rotor speed in different dynamic eccentricity (unbalance mass) cases using Method 2 (right), close-up near the 0.25 speed ratio (left).

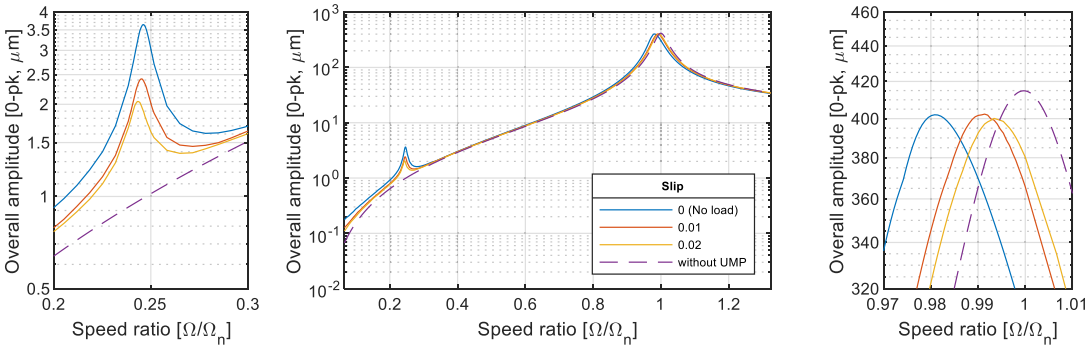

FIGURE 9. Vibration responses versus rotor speed in different slip cases with 30 % static eccentricity using Method 2 (center figure), close-up near the 0.25 speed ratio (left), and close-up near the critical speed (right).

vibration change with an increase in the unbalance mass is mainly caused by the centrifugal force. Thus, it can be concluded that the UMP caused by the dynamic eccentricity has no significant effect on the vibration amplification at the 0.25 speed ratio. This is probably explained by the fact that the UMP force caused by the dynamic eccentricity is much smaller than the UMP force caused by the static eccentricity.

Fig. 9 shows the vibration responses in different slip cases. It demonstrates that when the slip increases from 0 to 0.02, the reduction in the critical speed decreases. The reason for this is probably that the UMP force decreases with an increase in slip as shown in Table 2. By contrast, the peak response close to the 0.25 speed ratio occurs at a relatively low rotor speed when the slip increases. This is because this peak response occurs when the twice-line frequency excitation coincides with the mechanical natural frequency of the rotor. However, when the slip increases, the line frequency at the same rotor speed increases, and therefore, the resonance occurs at a relatively low rotor speed.

For investigation of the vibration excitations generated by the UMP, Fig. 10 and 11 show the rotor orbit and rotor displacements in the time and frequency domains at the 122 Hz supply frequency (near the 0.25 speed ratio) for cases with and without UMP. In particular, to investigate the effect of slip, results for two different slip cases: 0 and 0.02 are obtained. Firstly, the results show that higher frequency excitations are generated by the UMP, and specifically, a 4× speed frequency (twice the line frequency) component appears to be higher than the other harmonics. This is probably the main cause of the peak response at the 0.25 speed ratio and the three small circles in the fundamental circle as in the rotor orbit.

Considering the effect of slip, a comparison of the frequency domain displacements between no slip and 0.02 slip cases reveals a change in the electromagnetic excitation frequency when the slip is generated. First, the first harmonic frequency decreases because this harmonic is due to the whirling motion of the rotor, and its frequency decreases as the rotor speed decreases. Second, the fourth harmonic frequency remains unchanged because this harmonic comes from twice the line frequency excitation. Finally, two slightly different harmonics appear around the second, and third and fifth harmonic frequencies move toward the fourth harmonic frequency. Additionally, the results show that the slip reduces all the electromagnetic excitation magnitudes. Because of these changes in excitations, the rotor orbit becomes smaller in size and different in shape as shown in Fig. 10(d). The vibration of the rotor is generated from both the unbalance mass excitation and the UMP force excitation. However, in the presence of slip, twice the line frequency becomes slightly smaller than four times the whirling frequency. Therefore, the rotor orbit rotates around the center of whirling

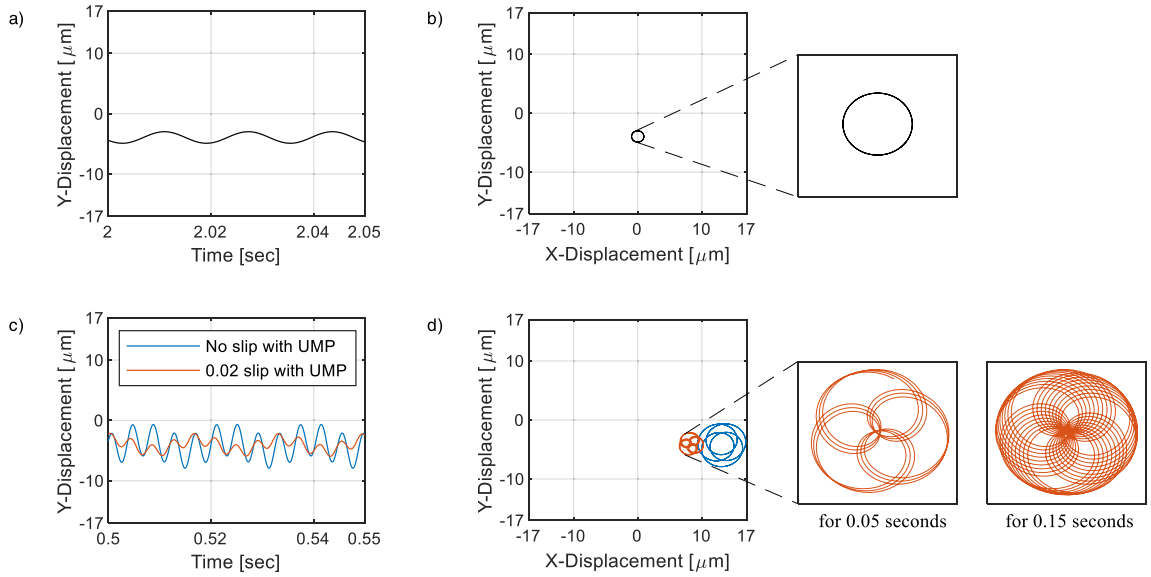

FIGURE 10. Time-domain displacement and rotor orbit at the 122 Hz supply frequency (near the 0.25 speed ratio) for three cases: without UMP and two different slip cases with UMP. a) Without UMP; time-domain displacement. b) Without UMP; rotor orbit. c) With UMP (two different slip cases); time-domain displacements. d) With UMP (two different slip cases); rotor orbits (left), rotor orbit for the 0.02 slip case in 0.05 s and 0.15 s (right).

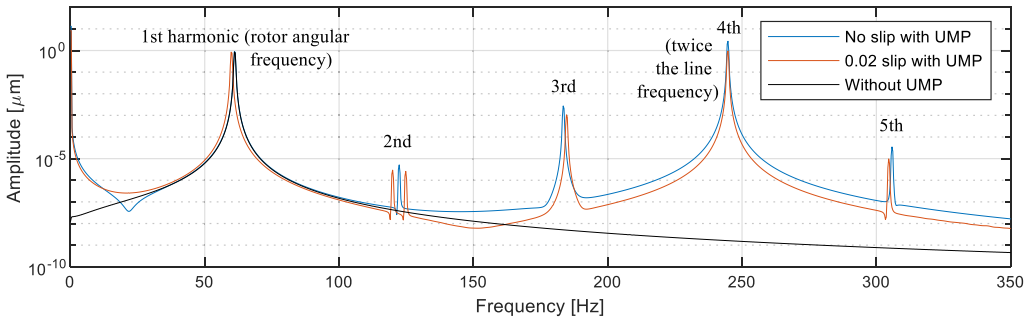

FIGURE 11. Frequency-domain displacement at the 122 Hz supply frequency (near the 0.25 speed ratio) for three cases: without UMP and two different slip cases with UMP.

motion as in Fig. 10(d) for the 0.02 slip case. This orbit is obtained in 0.05 s for about three rotations of the rotor. It is compared with the orbit during 0.15 s to determine the rotation of the orbit.

Fig. 12 presents the overall vibration amplitude for different bearing stiffness cases. It shows that the degree of the UMP effect for the induction motor depends on the structural properties of the rotor–bearing system. When the rotor–bearing system is less stiff, the UMP effect is more significant. When considering the actual operation of the machine under study, the UMP effect is not harmful to the system because the UMP-generated vibration appears at a rotor speed that is significantly above the operating range of the motor. However, when the bearing stiffness is 10^7 N/m, the UMP effect occurs within the operation range, rendering it harmful to the system.

Finally, Fig. 13 shows the vibration responses in different simulation methods. It shows that the UMP effect in Method 1 is stronger than the effect in Method 2 because

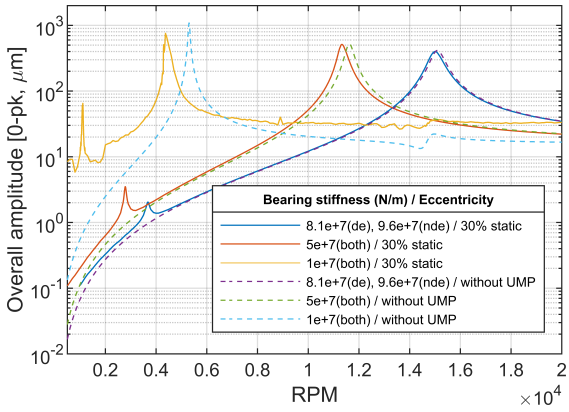

FIGURE 12. Vibration responses versus rotor speed in different bearing stiffness cases.

the UMP force calculated by Method 1 is higher than the result obtained by the FEA and Method 2. On the other hand, when investigating the result obtained by the linearized UMP

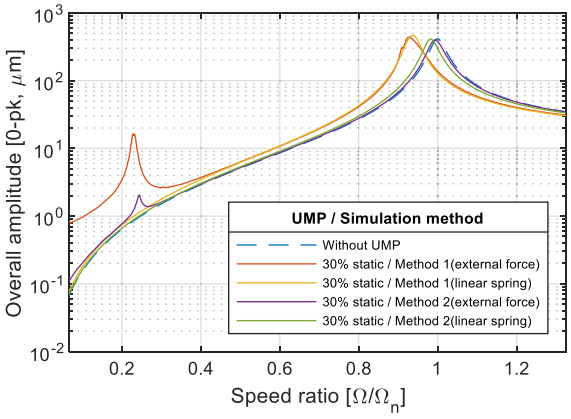

FIGURE 13. Vibration responses versus rotor speed in different simulation method cases.

negative stiffness spring model, it can be seen that the critical speed reduction effect appears to be slightly different with the result by time step analysis with Methods 1 and 2, and larger vibration at the 0.25 speed ratio is not detected unlike with the methods by time step analysis. Here, the UMP spring stiffnesses are calculated from the UMP force equations by Method 1 and 2, respectively.

Thus, when using Methods 1 and 2, two types of UMP effects can be observed. However, the degree of the effect is affected by the accuracy of the calculated UMP force. The method with the UMP spring model can only simulate the effect of critical speed reduction, and furthermore, this effect appears somewhat differently with the actual effect. Therefore, if only the variation in the critical speed is of interest and the error is within an acceptable range, this method can be employed as a simple simulation method. However, the acceptability of the error cannot be defined clearly, probably because the degree of error depends on the rotor–bearing system.

Based on the results obtained, a suggestion for the simulation strategy can be made. By using Method 1, the UMP force equation and the linearized UMP stiffness can be obtained by analytical calculation in the induction motor design process without extra cost. Further, if the rotordynamic simulation includes the use of the UMP stiffness, the result can be obtained quite easily. Therefore, this result can provide initial guidelines for the analysis of the UMP effect, even though there is an error in the UMP force amplitude. The obtained UMP effect is probably larger than the actual effect because the calculated UMP force is higher than the actual force, as shown in Table 2. Therefore, these guidelines can be taken as a criterion providing a safety margin in the initial design process. In pursuit of the final design, where accurate estimation of the UMP effect is required, simulation by the improved Method 2 and the time step analysis is advisable and the rotordynamic result can be updated for the final analysis.

IV. CONCLUSION

This study addressed the development of UMP force calculation methods for rotordynamic simulation. The proposed methods used the magnetizing current and included the effects of slot opening and saturation by including the Carter factor. Moreover, a correction factor was introduced and calculated by the FEA to improve the UMP force equation. Based on this model, a rotordynamic simulation process concerning the UMP force was designed into the induction motor design process, and the UMP effect on the rotordynamics of the induction motor was investigated. Moreover, the feasibility of the proposed methods was discussed. The main findings of the study can be summarized as follows:

1) By the developed analytical UMP calculation model, the UMP force resulting from the air-gap eccentricity was calculated and compared with the FEA result. By using the magnetizing current and the correction factor obtained by the FEA, the analytical UMP force equation was improved.
2) The negative stiffness effect of the UMP reduces the critical speed of the rotor system. This effect results mainly from the dynamic eccentricity, whereas the reduction caused by the static eccentricity is negligible.
3) The results for the rotor displacement in the frequency domain show that the vibration components with the 2Ω, 3Ω, 4Ω, 5Ω frequencies are generated by UMP. Specifically, twice the line frequency excitation (4Ω in the case of a four-pole machine) leads to a higher vibration when it coincides with the natural frequency of the rotor. Hence, in the four-pole machine under study, a higher vibration appears at one-fourth of the critical speed. Moreover, this excitation is amplified by the static eccentricity but not by the dynamic eccentricity.
4) The results obtained for different values of bearing stiffness show that the degree of the UMP effect depends on the rotor–bearing system. A less stiff rotor-bearing system results in a greater effect of the UMP.
5) The simulation method applying the pure analytical UMP calculation and the linearized UMP stiffness can be used as a rough guideline in the initial stage of the induction motor design process. An improved simulation method supported by the FEA can be employed in the final stage requiring accurate estimation of the UMP effect in the induction motor design process.

REFERENCES

[1] H. Kim, A. Posa, J. Nerg, J. Heikkinen, and J. Sopanen, "Analysis of electromagnetic excitations in an integrated centrifugal pump and permanent magnet synchronous motor," *IEEE Trans. Energy Convers.*, vol. 34, no. 4, pp. 1759–1768, Dec. 2019.
[2] X. Sun, B. Su, S. Wang, Z. Yang, G. Lei, J. Zhu, and Y. Guo, "Performance analysis of suspension force and torque in an IBPMSM with V-Shaped PMs for flywheel batteries," *IEEE Trans. Magn.*, vol. 54, no. 11, pp. 1–4, Nov. 2018.
[3] X. Sun, Z. Jin, S. Wang, Z. Yang, K. Li, Y. Fan, and L. Chen, "Performance improvement of torque and suspension force for a novel five-phase BFSPM machine for flywheel energy storage systems," *IEEE Trans. Appl. Supercond.*, vol. 29, no. 2, Mar. 2019, Art. no. 0601505.
[4] R. P. Jastrzebski, P. Jaatinen, H. Sugimoto, O. Pyrhönen, and A. Chiba, "Design of a bearingless 100 kW electric motor for high-speed applications," in *Proc. 18th Int. Conf. Electr. Mach. Syst. (ICEMS)*, Oct. 2015, pp. 2008–2014.

[5] D. G. Dorrell, W. T. Thomson, and S. Roach, "Analysis of airgap flux, current, and vibration signals as a function of the combination of static and dynamic airgap eccentricity in 3-phase induction motors," *IEEE Trans. Ind. Appl.*, vol. 33, no. 1, pp. 24–34, Jan./Feb. 1997.
[6] D. G. Dorrell, "Sources and characteristics of unbalanced magnetic pull in three-phase cage induction motors with axial-varying rotor eccentricity," *IEEE Trans. Ind. Appl.*, vol. 47, no. 1, pp. 12–24, Feb. 2011.
[7] A. Tenhunen, T. Benedetti, T. P. Holopainen, and A. Arkkio, "Electromagnetic forces in cage induction motors with rotor eccentricity," in *Proc. IEEE Int. Electr. Mach. Drives Conf.*, Jun. 2003, pp. 1616–1622.
[8] A. Tenhunen, T. P. Holopainen, and A. Arkkio, "Impulse method to calculate the frequency response of the electromagnetic forces on whirling cage rotors," *IEE Proc.-Electr. Power Appl.*, vol. 150, no. 6, pp. 752–756, Nov. 2003.
[9] A. Tenhunen, T. P. Holopainen, and A. Arkkio, "Effects of equalizing currents on electromagnetic forces of whirling cage rotor," in *Proc. IEEE Int. Electr. Mach. Drives Conf.*, Jun. 2003, pp. 257–263.
[10] A. Tenhunen, T. P. Holopainen, and A. Arkkio, "Effects of saturation on the forces in induction motors with whirling cage rotor," *IEEE Trans. Magn.*, vol. 40, no. 2, pp. 766–769, Mar. 2004.
[11] T. P. Holopainen, A. Tenhunen, and A. Arkkio, "Electromechanical interaction in rotordynamics of cage induction motors," *J. Sound Vib.*, vol. 284, nos. 3–5, pp. 733–755, 2005.
[12] P. Frauman, A. Burakov, and A. Arkkio, "Effects of the slot harmonics on the unbalanced magnetic pull in an induction motor with an eccentric rotor," *IEEE Trans. Magn.*, vol. 43, no. 8, pp. 3441–3444, Aug. 2007.
[13] B. Silwal, P. Rasilo, and A. Arkkio, "Prospects and limitations of power balance approach for studying forces and electromagnetic damping in electrical machines," *IEEE Trans. Magn.*, vol. 54, no. 2, Feb. 2018, Art. no. 8100708.
[14] X. Han and A. Palazzolo, "Unstable force analysis for induction motor eccentricity," *J. Sound Vib.*, vol. 370, pp. 1–464, May 2016.
[15] C. Di, X. Bao, H. Wang, Q. Lv, and Y. He, "Modeling and analysis of unbalanced magnetic pull in cage induction motors with curved dynamic eccentricity," *IEEE Trans. Magn.*, vol. 51, no. 8, Aug. 2015, Art. no. 8106507.
[16] J. Nerg, J. Pyrhonen, and J. Partanen, "Finite element modeling of the magnetizing inductance of an induction motor as a function of torque," *IEEE Trans. Magn.*, vol. 40, no. 4, pp. 2047–2049, Jul. 2004.
[17] M. Berman, "On the reduction of magnetic pull in induction motors with off-centre rotor," in *Proc. Conf. Rec. IEEE Ind. Appl. Conf. 28th IAS Annu. Meeting*, Oct. 1993, pp. 343–350.
[18] B. Heller and V. Hamata, *Harmonic Field Effects in Induction Machines*. Amsterdam, The Netherlands: Elsevier, 1977.
[19] J. Pyrhönen, T. Jokinen, and V. Hrabovcova, *Design of Rotating Electrical Machines*, 2nd ed. Hoboken, NJ, USA: Wiley, 2014.
[20] W. R. Finley, M. M. Hodowanec, and W. G. Holter, "An analytical approach to solving motor vibration problems," *IEEE Trans. Ind. Appl.*, vol. 36, no. 5, pp. 1467–1480, Sep./Oct. 2000.
[21] E. P. J. Gargiulo, "A simple way to estimate bearing stiffness," *Mach. Design*, vol. 52, no. 17, pp. 107–110, 1980.
[22] E. Krämer, *Dynamics of Rotors and Foundations*. Berlin, Germany: Springer-Verlag, 1993.

HEESOO KIM was born in Seoul, South Korea, in 1979. He received the B.S. and M.S. degrees in mechanical engineering from Hanyang University, Seoul, in 2005 and 2007, respectively. He is currently pursuing the Ph.D. degree with the Department of Mechanical Engineering, LUT University, Lappeenranta, Finland. He was a turbocharger development engineer for marine and vehicle engines. His research interest includes rotordynamics for electrical machines, specifically the studies about electromechanical interaction from air gap eccentricity, stator deformation, and other geometric non-idealities.

JANNE NERG (Senior Member, IEEE) received the M.Sc. degree in electrical engineering, the Licentiate of Science (technology) degree, and the D.Sc. (technology) degree from LUT University, Lappeenranta, Finland, in 1996, 1998, and 2000, respectively. He is currently an Associate Professor with the Department of Electrical Engineering, LUT University. His research interests include electrical machines and drives, especially electromagnetic and thermal modeling, and the design of electromagnetic devices.

TUHIN CHOUDHURY was born in Seppa, India, in 1989. He received the B.Sc. (tech) degree in mechanical engineering from Sikkim Manipal University, India, in 2011, and the M.Sc. degree in mechatronic system design from LUT University, Lappeenranta, Finland, in 2018, where he is currently pursuing the Ph.D. degree with the Department of Mechanical Engineering. He was a design engineer on the development of medical devices and diagnostic instruments, from 2011 to 2016. His research interests include designing, modeling, and simulation of rotating machines, and the analysis of rotor behavior to understand the root cause of unwanted vibrations, specifically due to unbalance.

JUSSI T. SOPANEN (Member, IEEE) was born in Enonkoski, Finland, in 1974. He received the M.Sc. degree in mechanical engineering and the D.Sc. (technology) degree from LUT University, Lappeenranta, Finland, in 1999 and 2004, respectively. He was a Researcher with the Department of Mechanical Engineering, LUT University, from 1999 to 2006. He was a Product Development Engineer of electric machine manufacturing with Rotatek Finland Ltd. from 2004 to 2005. From 2006 to 2012, he was a Principal Lecturer in mechanical engineering and the Research Manager of the Faculty of Technology, Saimaa University of Applied Sciences, Lappeenranta. He is currently serving as a Professor with the Machine Dynamics Laboratory, LUT University. His research interests include rotor dynamics, multibody dynamics, and the mechanical design of electrical machines.